Journal of Molecular Modeling (2024) 30:118
https://doi.org/10.1007/s00894-024-05910-7

ORIGINAL PAPER

Investigation of second-order NLO properties of novel 1,3,4-oxadiazole derivatives: a DFT study

Balachandar Waddar[1] · Suman Gandi[1] · Saidi Reddy Parne[1] · Vishnu Rama Chari[2] · Gurusiddappa R. Prasanth[3]

Received: 29 January 2024 / Accepted: 20 March 2024 / Published online: 2 April 2024

Abstract

Context In this study, we have developed four new chromophores (TM1–TM4) and performed quantum chemical calculations to explore their nonlinear optical properties. Our focus was on understanding the impact of electron-donating substituents on 1,3,4-oxadiazole derivative chromophores. The natural bond orbital analysis confirmed the interactions between donors and acceptors as well as provided insights into intramolecular charge transfer. We also estimated dipole moment, linear polarizability molecular electrostatic potential, UV–visible spectra, and first hyperpolarizability. Our results revealed that TM1 with a strong and stable electron-donating group exhibited high first hyperpolarizability (β) 293,679.0178 × 10^{-34} esu. Additionally, TM1 exhibited a dipolar moment (μ) of 5.66 Debye and polarizability (α) of 110.62 × 10^{-24} esu when measured in dimethyl sulfoxide (DMSO) solvent. Furthermore, in a benzene solvent, TM1 showed a low energy band gap of 5.33 eV by using the ωB97XD functional with a 6–311 + + G(d, p) basis set. Moreover, our study of intramolecular charge transfers highlighted N, N dimethyl triphenylamine and carbazole as major electron-donating groups among the four 1,3,4-oxadiazole derivative chromophores. This research illustrates the potential applications of these organic molecules in photonics due to their versatile nature.

Methods The molecules were individually optimized using different functionals, including APFD, B3LYP, CAM B3LYP, and ωB97XD combined with the 6–311 + + G (d, p) basis set in Gaussian 16 software. These methods encompass long-range functionals such as APFD and B3LYP, along with long-range corrected functionals like CAM B3LYP and ωB97XD. The employed functionals of APFD, B3LYP, CAM B3LYP, and ωB97XD with the 6–311 + + G (d,p) basis set were used to extract various properties such as geometrical structures, dipole moment, molecular electrostatic potential, and first hyperpolarizability through precise density functional theory (DFT). Additionally, TD-DFT was utilized for obtaining UV–visible spectra. All studies have been conducted in both gas and solvent phases.

Keywords Nonlinear optical materials · 1,3,4-oxadiazoles · First hyperpolarizability · NBO · HOMO LUMO · ICT · Density functional theory (DFT) · TD DFT

Introduction

Organic materials received much more importance in the emerging field of nonlinear optics [1–3], due to their promising structural, optical, and strong intramolecular charge transfer (ICT) properties. These have been known for their low cost, ease of processing, and larger electro-optical coefficients as compared to inorganic materials [4–6]. Organic materials have a large number of applications in photonics such as optical data processing, optical data storage, optical communication switches, and cloud computing [7–9]. With the help of the materials researcher's efforts, a large class of organic second-order NLO materials have been introduced in recent years to achieve the expected

✉ Saidi Reddy Parne
psreddy@nitgoa.ac.in

[1] Department of Applied Sciences, National Institute of Technology Goa, Kottamoll Plateau, Cuncolim, Goa 403703, India

[2] School of Chemical Sciences, Goa University, Taleigao Plateau, Goa 403206, India

[3] Department of Electronics & Communication Engineering, National Institute of Technology Goa, Kottamoll Plateau, Cuncolim, Goa 403703, India

first hyperpolarizability. The first hyperpolarizability is the key factor for second-ordered NLO materials particularly optoelectronic applications [10, 11]. The most effective way of achieving the first hyperpolarizability is by choosing conjugated π systems by introducing a combination of strong electron donating and withdrawing groups by limited chain length [12]. Organic materials studied extensively confirm that with π conjugated push–pull type system is feasible to modulate for their optical, electronic, and chemical properties by adapting their molecular structure [13]. Higher NLO properties have been demonstrated by D-π-A type NLO organic chromophores. Here, D and A stand for functional groups that donate and accept electrons, respectively, while π denotes a conjugated bridge interaction through π-π* bonds that promote charge transfer and increase NLO activity [14].

Amidst the variety of organic molecules important for nonlinear optical (NLO) applications, certain compounds with strong electron-withdrawing characteristics like 1,3,4-oxadiazoles, thiosemicarbazones, imidazolium, and benzimidazoles are notable due to their exceptional second- and third-order NLO responses. These molecular frameworks display high NLO activity because of their significant ability to facilitate charge transfer within their structure—a crucial feature for NLO materials. A recent study has highlighted the considerable attention garnered by derivatives of 1,3,4-oxadiazoles across diverse fields such as optoelectronics and medicinal chemistry compounds along with dye-sensitized solar cells (DSSC) [15–17]. These derivatives are part of the heterocyclic moiety, belonging to the family of organic compounds with significant electron transport properties, high thermal ability, oxidative stability, and strong electron-withdrawing properties. They also exhibit strong fluorescence with good quantum yield, making them valuable in the development of materials for electroluminescent applications and electron-transporting materials [18, 19]. The study highlights the increasing focus on pharmaceutical, optical, biological, optoelectronic, and OLED applications of 1,3,4-oxadiazole derivatives while noting a limited number of works reported on their second nonlinear optical properties. S.S. Oliveira and colleagues investigated the use of different group molecules with 1,3,4-oxadiazoles, reporting second-order NLO properties with a first hyperpolarizability (β) of 24.0×10^{-30} esu [20]. Khemalapure et al. conducted research on the spectroscopic, optical, and NLO properties of 1,3,4-oxadiazole derivatives [21]. Alongamo et al. studied the impact of substituents on the charge transport and nonlinear optical (NLO) properties of 1,3,4-oxadiazole derivatives [22]. Carella et al. explored the use of thiophene rings with 1,3,4-oxadiazole chromophores for second-order NLO properties [23]. Yi-Kai Fang et al. focused on non-conjugated random copolymers with pendant electron-donating 1,3,4-oxadiazole derivative moieties [24]. Homocianu et al. conducted a study and review of fluorinated 1,3,4-oxadiazole derivatives, examining their NLO parameters [25]. In a study by Dhannur et al., advanced DFT methods were used to investigate the NLO properties of D–π–A substituted bis-1,3,4-oxadiazoles [26]. The synthesized molecules were both structurally confirmed through spectroscopic techniques and showed significant NLO activity, with hyperpolarizability values exceeding that of standard benchmarks like urea by 55 times. These exceptional characteristics highlight the potential usefulness of these compounds in NLO applications. Additionally, the research conducted by Homocianu et al. delved into the nonlinear optical properties and metal ion sensing capabilities of a polymer composed of 1,3,4-oxadiazole and bisphenol A units. Utilizing UV–Vis absorption and fluorescence spectroscopies, the solvatochromic method revealed this polymer's significant NLO parameters ($\alpha=0.54\times10^{-23}$ esu, $\beta=2.99\times10^{-29}$ esu, and $\gamma=9.21\times10^{-34}$ esu) [27]. Another study by Silva et al. investigated two 1,3,4-oxadiazole derivatives, demonstrating their substantial second-order optical nonlinearity as seen in their first hyperpolarizability values (106×10^{-34} esu and 126×10^{-34} esu) [28]. These findings collectively underscore the potential of these compounds for advanced optoelectronic applications.

The role of NLO materials is crucial in modern photonic applications, but the challenge lies in finding new compounds with strong NLO response, good thermal stability, and easy processing. Employing the density functional theory method offers significant advantages in designing materials and estimating their potential electronic, optical, and NLO properties [29]. This study aimed to investigate the second-order NLO properties of novel 1,3,4-oxadiazole derivatives using DFT. The specific objectives were to design a series of D-π-A type push–pull chromophores based on 1,3,-4-oxadiazole derivatives; evaluate the impact of different donor groups on the NLO properties of these chromophores; and identify structure–property relationships that may lead to materials with enhanced NLO performance. To achieve this goal, a set of four D-π-A type push–pull 1,3,4-oxadiazole derivative chromophores (Fig. 1) were designed, namely (Z)-4-(5-(4-(bis(4-(dimethylamino) phenyl)amino)styryl)-1,3,4-oxadiazol-2-yl)phthalonitrile, (E)-4-(5-(2-(10-propyl-10H-phenothiazin-3-yl)vinyl)-1,3,4-oxadiazol-2-yl)phthalonitrile, (E)-4-(5-(2-(anthracen-9-yl)vinyl)-1,3,4-oxadiazol-2-yl) phthalonitrile, and (E)-4-(5-(4-(9H-carbazol-9-yl)styryl)-1,3,4-oxadiazol-2-yl) phthalonitrile are abbreviated as TM1, TM2, TM3, and TM4 to achieve second-order NLO properties. Additionally, a series of donors including triphenylamine, phenothiazine, anthracene, and carbazole, together with 1,3,4-oxadiazole as a common withdrawing group, were employed to attain exceptional second-order NLO properties. These substituents were chosen due to their robust electron-donating capabilities, which are well-documented in the literature [30–35].

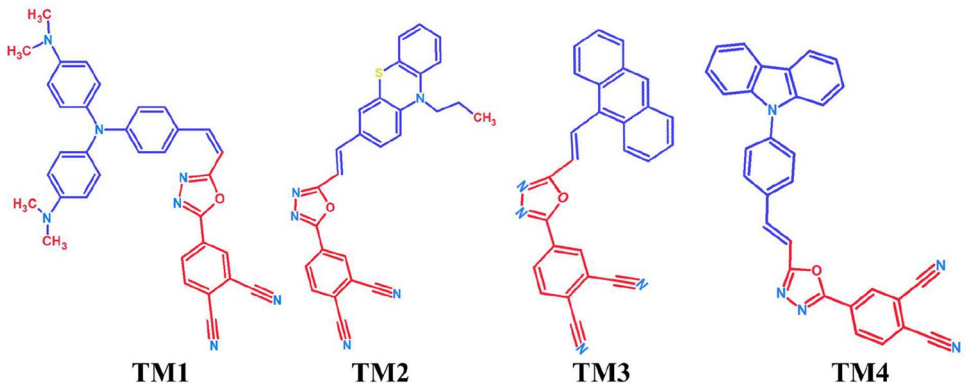

Fig. 1 1,3,4-oxadiazole derivative chromophores TM1, TM2, TM3, and TM4

The rationale behind the selection is rooted in their ability to enhance the electron density on the conjugated 1,3,4-oxadiazole core, thereby having the potential to improve the second-order nonlinear optical (NLO) properties of the molecules. Triphenylamine is known for its strong electron-donating nature and its stability, which makes it an excellent candidate for electronic applications [35]. Carbazole is a heteroaromatic compound recognized for its high thermal stability and favorable electronic properties [34]. Carbazole and triphenylamine units are commonly utilized in organic donor materials due to their outstanding optical and electronic properties. The carbazole structure can be extensively modified and is widely used in applications such as organic light-emitting diodes [36, 37]. Phenothiazine provides a unique combination of electron donation capability and steric hindrance that influences molecular packing and electron transport [31]. Additionally, phenothiazine units with strong electron-donating capacity have distinct electronic properties; these have been frequently utilized as donor groups in dye-sensitized solar cells (DSSCs). Anthracene, a polycyclic aromatic hydrocarbon, contributes to extended π-conjugation, potentially increasing NLO responses [32]. Each donor was carefully chosen to explore the effects of different electronic and steric properties on the overall NLO performance of the 1,3,4-oxadiazole derivatives. These substituents not only enhance the intramolecular charge transfer but also contribute to the structural diversity of the compounds, thus offering a broad perspective on structure–property relationships in the context of NLO materials.

Computational method

In this investigation, the quantum chemical calculations were carried out using the Gaussian 16 program suite [38]. Density functional theory (DFT) was employed for all calculations. Initially, the geometries of chromophores TM1-TM4 were optimized in C1 symmetry using DFT functionals APFD, B3LYP, CAM-B3LYP, and ωB97XD. The choice of APFD and B3LYP functionals was based on their proven reliability in accurately predicting electronic properties across a wide range of molecular systems. Specifically, APFD is known for its balanced treatment of exchange–correlation energy while B3LYP demonstrates general-purpose applicability across diverse chemical systems. For long-range corrected functionals, CAM-B3LYP and ωB97XD were selected to account for significant long-range electron–electron interactions crucial in studying NLO properties. CAM-B3LYP allows tunable range-separation parameters important for studies involving charge transfer states while ωB97XD incorporates dispersion corrections making it adept at modeling non-covalent interactions—an essential factor given our novel 1,3,4-oxadiazole derivatives. By combining these functions, we aimed to achieve a comprehensive analysis ensuring reliability of geometric structures. Moreover, the complementary strengths of these functionals, each meticulously chosen for their proven competencies in different aspects of DFT calculations, coalesce to offer an in-depth and accurate understanding of the second-order NLO properties that are central to our study's objectives. Further stability analysis was conducted for each wavefunction in the gas phase, with no imaginary frequency found due to the various degrees of freedom of both structure and wavefunction. To examine the nonlinear optical (NLO) behavior and other associated intramolecular charge transfer properties of chromophores TM1–TM4, electrical properties such as dipole moment (μ), polarizability (α), first hyperpolarizability (β), natural bond orbital analysis (NBO), and frontier molecular orbitals (FMO) for the ground state were estimated using the time-independent DFT method. A time-dependent TD-DFT method was utilized to approximate vertical energy transitions for the UV–visible spectra. The estimated properties were derived from both the gaseous phase and five different solvent environments, including acetonitrile, benzene, dichloromethane (DCM), dimethyl sulfoxide (DMSO), and ethanol. The influence of solvents was investigated using the universal solvent model (SMD) [39]. This model efficiently captures polarization effects by

considering the dielectric constant and surface tension of the solvent, resulting in a more precise simulation of real-life conditions where the NLO properties would be observed. Throughout the study, the 6–311 + + G (d, p) level basis set with functionals was utilized to enhance precision and provide a detailed representation of molecular orbitals. In this basis set, the polarization of hydrogen atoms is indicated by d, while all other heavy atoms are represented by p.

Results and discussion

Dipole moment

The static dipole moment is greatly influenced by the structure and the electronegativity of the atoms present in the structure, as well as the induced field [40]. The influence of a polar solvent is also taken into consideration. Using the same level theory, the ground state dipole moment of chromophores TM1–TM4 is estimated. Generally, the dipole moment increases as the polarity of the solvents increases. The dipole moment values for TM1–TM4 are calculated using Eq. (1) and are presented in Table 1, 2, 3, and 4. The order of dipole moment values for TM1–TM4 is TM1 > TM2 > TM4 > TM3.

$$\text{Dipole moment, } \mu = \left(\mu_x^2 + \mu_y^2 + \mu_z^2\right)^{\frac{1}{2}} \text{ in Debye} \quad (1)$$

The effect of donor functional groups and solvents on all the molecules is evident in the dipole moment values. A higher dipole moment value is observed in TM1 due to the substitution of the triphenylamine functional group, which donates a greater number of partial charges from the donor end. TM2 and TM4 also exhibit moderate donation of partial charges, attributed to the phenothiazine and carbazole functional groups. Conversely, TM3 shows a lower dipole moment value upon substitution of anthracene, as its flat structure contributes to a low partial charge donation compared to other chromophores. Additionally, the dipole moment values increase in solvents, with remarkable values observed in DMSO, following the order of solvent polarity index [41].

Linear polarizability

The linear polarizability (α), also referred to as the first-order NLO response, represents the system's reaction to an applied electric field [42]. It is associated with intramolecular charge transfer (ICT). When an external electric field interacts with the surplus electrons in these systems, it amplifies the dipole moments, thereby elevating the linear

Table 1 Calculated dipole moment (μ) in Debye, polarizability (α) (in 10^{-24} esu), and first hyperpolarizability (β) (in 10^{-34} esu) at 6–311 + + G (d, p) level basis set for TM1

Gas				Solvent			
Functional	μ (in Debye)	α (10^{-24} esu)	β (10^{-34} esu)		μ (in Debye)	α (10^{-24} esu)	β (10^{-34} esu)
APFD	5.656915275	92.57449805	684,874.0051	Acetonitrile	6.525676831	128.6448126	1,418,404.302
				Benzene	6.18694704	108.1409343	1,115,348.318
				DCM	6.463941243	122.9671738	1,371,883.315
				DMSO	6.543499283	129.1987914	1,430,799.79
				Ethanol	6.483288577	127.6923927	1,391,785.541
B3LYP	5.964357304	94.04360488	718,867.5922	Acetonitrile	6.961000945	130.7435151	1,527,947.643
				Benzene	6.546190255	109.9044744	1,192,029.721
				DCM	6.877887993	124.9840485	1,477,289.297
				DMSO	6.980179484	131.3108816	1,541,961.428
				Ethanol	6.917459552	129.7790206	1,499,537.741
CAM B3LYP	5.075833058	81.2780704	2,081,110.4077	Acetonitrile	5.770678906	110.5025648	13,570,888,673
				Benzene	5.487510731	93.0465733	284,689.1525
				DCM	5.716142321	105.4483815	331,301.5379
				DMSO	5.785352927	110.9482837	344,264.0797
				Ethanol	5.737906282	109.7680578	338,632.303
ωB97XD	4.970521381	80.80797773	178,565.4547	Acetonitrile	5.646734512	110.1741953	292,221.684
				Benzene	5.368994323	92.53231709	242,337.5547
				DCM	5.592708052	105.0360819	282,453.237
				DMSO	5.661639924	110.6229904	293,679.0178
				Ethanol	5.614068287	109.437225	289,247.5797

Table 2 Calculated dipole moment (μ) in Debye, polarizability (α) (in 10^{-24} esu), and first hyperpolarizability (β) (in 10^{-34} esu) at 6–311 + + G (d, p) level basis set for TM2

Gas				Solvent			
Functional	μ (in Debye)	α (10^{-24} esu)	β (10^{-34} esu)		μ (in Debye)	α (10^{-24} esu)	β (10^{-34} esu)
APFD	3.906145452	71.18572408	278,029.0844	Acetonitrile	4.395087572	98.16928154	581,989.6119
				Benzene	4.21751177	82.5307672	439,379.3586
				DCM	4.366423025	93.84045153	553,854.2528
				DMSO	4.401214231	98.56918209	587,261.9838
				Ethanol	4.378560421	97.45866235	568,878.4239
B3LYP	3.913528698	72.64927624	306,673.7491	Acetonitrile	4.41663455	100.5350062	660,140.5319
				Benzene	4.234772549	84.40563726	492,641.5994
				DCM	4.387607871	96.08120408	626,721.5188
				DMSO	4.423089642	100.9510802	666,326.8747
				Ethanol	4.399264806	99.7895364	644,835.2726
CAM B3LYP	3.472894589	64.24249118	112,795.0372	Acetonitrile	3.830072501	87.30876912	193,940.1775
				Benzene	3.700052845	73.58966682	158,309.5462
				DCM	3.808553993	83.41698638	186,900.8782
				DMSO	3.834001522	87.65214973	195,477.3838
				Ethanol	3.820713867	86.72749476	189,828.3945
ωB97XD	3.43359274	63.93808397	96,552.52168	Acetonitrile	Acetonitrile	3.782430099	87.09072033
				Benzene	Benzene	3.654976405	73.25709335
				DCM	DCM	3.761383733	83.14697489
				DMSO	DMSO	3.786069461	87.43539356
				Ethanol	Ethanol	3.774125975	86.51337471

Table 3 Calculated dipole moment (μ) in Debye, polarizability (α) (in 10^{-24} esu), and first hyperpolarizability (β) (in 10^{-34} esu) at 6–311 + + G (d, p) level basis set for TM3

Gas				Solvent			
Functional	μ (in Debye)	α (10^{-24} esu)	β (10^{-34} esu)		μ (in Debye)	α (10^{-24} esu)	β (10^{-34} esu)
APFD	2.835043094	72.6488499	236,941.0927	Acetonitrile	3.168462768	100.1772019	379,844.3082
				Benzene	3.060610009	84.04385216	327,936.5531
				DCM	3.15585538	95.65959439	372,588.0655
				DMSO	3.175203187	100.5840353	382,998.848
				Ethanol	3.153405409	99.47998216	372,279.9919
B3LYP	2.825994249	73.82588179	255,935.4009	Acetonitrile	3.17767039	101.9501069	411,776.941
				Benzene	3.058611538	85.4704096	354,993.169
				DCM	3.161902417	97.33545224	403,713.2249
				DMSO	3.184652381	102.3694692	415,387.9149
				Ethanol	3.162710631	101.2305314	403,556.6419
CAM B3LYP	2.559139809	65.91589317	85,094.02962	Acetonitrile	2.848886977	90.51155045	123,298.1606
				Benzene	2.747550527	75.79551955	110,629.9766
				DCM	2.834872587	86.32514253	121,781.3485
				DMSO	2.854947071	90.87333641	124,222.5526
				Ethanol	2.835881546	89.90508136	121,101.74
ωB97XD	2.527016124	65.7275624	72,171.88172	Acetonitrile	2.816099096	90.55912113	104,561.1828
				Benzene	2.714940245	75.65287781	93,869.20438
				DCM	2.802313308	86.30503364	103,323.8379
				DMSO	2.822072383	90.92382203	105,306.3838
				Ethanol	2.802854429	89.95031999	102,712.9757

Table 4 Calculated dipole moment (μ) in Debye, polarizability (α) (in 10^{-24} esu), and first hyperpolarizability (β) (in 10^{-34} esu) at 6–311 + + G (d, p) level basis set for TM4

Gas				Solvent			
Functional	μ (in Debye)	α (10^{-24} esu)	β (10^{-34} esu)		μ (in Debye)	α (10^{-24} esu)	β (10^{-34} esu)
APFD	3.088552215	60.4586149	128,571.0189	Acetonitrile	3.607023251	87.73741809	247,432.7184
				Benzene	3.391692455	71.57637194	197,780.7412
				DCM	3.567453638	83.22301837	239,267.6528
				DMSO	3.613037037	88.13572466	249,829.4094
				Ethanol	3.592146224	87.05482994	241,387.9769
B3LYP	3.140793139	61.7668004	145,373.1205	Acetonitrile	3.678499225	89.90927415	291,257.6586
				Benzene	3.455654278	73.25976961	228,462.4054
				DCM	3.637488197	85.26617106	280,443.0504
				DMSO	3.685109915	90.32171762	294,183.6345
				Ethanol	3.66285037	89.19421961	283,904.143
CAM B3LYP	2.862341311	55.60551142	45,939.39056	Acetonitrile	3.322753791	79.74244006	77,034.70233
				Benzene	3.122761311	65.24451156	64,371.82235
				DCM	3.28401923	75.64522947	74,808.29039
				DMSO	3.327597734	80.09208816	77,685.03903
				Ethanol	3.311096615	79.16497472	75,468.94047
ωB97XD	2.80011183	55.31493074	37,060.18502	Acetonitrile	3.261120646	79.52523096	61,784.27212
				Benzene	3.057162781	64.93012449	51,676.28543
				DCM	3.22088405	75.38267751	60,008.94205
				DMSO	3.265819314	79.87583749	62,252.26967
				Ethanol	3.250121443	78.94992024	60,653.44855

polarizability and first-order hyperpolarizability, which can be calculated using Eq. (2).

$$\alpha = \left(\frac{1}{3}\right)\left[\alpha_{xx} + \alpha_{yy} + \alpha_{zz}\right] \text{ esu} \tag{2}$$

Tables 1, 2, 3, and 4 display the α values for compounds TM1 to TM4. It is evident that the α value for TM4 is $55.31493074 \times 10^{-24}$ esu in the gaseous phase and $79.87583749 \times 10^{-24}$ esu in DMSO, which represents the lowest value among the estimated series of compounds. In contrast, TM1 exhibits the most polarizable nature, with significantly higher values of $80.80797773 \times 10^{-24}$ esu in the gaseous phase and $110.6229904 \times 10^{-24}$ esu in DMSO. Meanwhile, TM2 and TM3 demonstrate α values of $63.93808397 \times 10^{-24}$ esu and $65.7275624 \times 10^{-24}$ esu in the gaseous phase, and $87.43539356 \times 10^{-24}$ esu and $90.92382203 \times 10^{-24}$ esu in DMSO, respectively. Overall, the compounds exhibit comparable α values, with the trend being TM1 > TM3 > TM2 > TM4 in both gaseous and solvent phases.

First hyperpolarizability

The first hyperpolarizability is a third-rank tensor represented by a $3 \times 3 \times 3$ matrix. This matrix contains 27 components, which can be reduced to 10 components due to Kleinman symmetry. The first hyperpolarizability is a key factor in determining the strength of second-order nonlinear optical (NLO) materials [43]. The static first hyperpolarizability of the designed molecules TM1–TM4 has been computed using Eq. (3) to analyze their NLO responses, and the results are presented in Table 1, 2, 3, and 4. Initially, we estimated the first hyperpolarizability of TM1–TM4 molecules using the four hybrid functionals mentioned above, both in gas and in five solvents using the solvatochromic method. The results indicated that the order of first hyperpolarizability is TM1 > TM2 > TM3 > TM4 and the first hyperpolarizability increases as the polarity of the solvents increases.

$$\beta_{\text{total}} = \left[\left(\beta_{xxx} + \beta_{xyy} + \beta_{xzz}\right)^2 + \left(\beta_{yyy} + \beta_{xxy} + \beta_{yyz}\right)^2 + \left(\beta_{zzz} + \beta_{xxz} + \beta_{yyz}\right)^2\right]^{\frac{1}{2}} \tag{3}$$

Due to the substitution of a dimethyl-attached triphenylamine functional group as a donor, the first hyperpolarizability value is higher in TM1. This is attributed to the greater contribution of charges from the lone pair of electrons from nitrogen and methyl groups. The molecule has a good donating capacity among all four molecules. Additionally, TM2 and TM3 are attached with phenothiazine and anthracene respectively, both are good donors due to their donating capacity, resulting in a lower contribution of charges compared to TM1. Furthermore, the first

Table 5 Chemical hardness (η) (in eV), chemical softness (σ) (in eV), HOMO, and LUMO (in au) for $\pi \rightarrow \pi^*$ interactions calculated at ωB97XD/6–311 + + G (d, p)

Gas						Solvent					
Molecule	Chemical hardness	Chemical softness	HOMO (eV)	LUMO (eV)	Energy gap (eV)		Chemical hardness	Chemical softness	HOMO (eV)	LUMO (eV)	Energy gap (eV)
TM1	2.68	0.37	− 6.59	− 1.23	5.36	Acetonitrile	2.7289	0.3664	− 6.52	− 1.06	5.46
						Benzene	2.6655	0.3752	− 6.48	− 1.15	5.33
						DCM	2.7066	0.3695	− 6.49	− 1.08	5.41
						DMSO	2.7288	0.3665	− 6.52	− 1.06	5.46
						Ethanol	2.7318	0.3661	− 6.51	− 1.05	5.46
TM2	3.08	0.32	− 7.72	− 1.35	6.17	Acetonitrile	3.0942	0.3232	− 7.25	− 1.06	6.19
						Benzene	3.0584	0.3270	− 7.33	− 1.21	6.12
						DCM	3.0799	0.3247	− 7.26	− 1.10	6.16
						DMSO	3.0934	0.3233	− 7.25	− 1.07	6.19
						Ethanol	3.0980	0.3228	− 7.25	− 1.05	6.20
TM3	3.13	0.32	− 7.73	− 1.47	6.26	Acetonitrile	3.2165	0.3109	− 7.52	− 1.08	6.43
						Benzene	3.1447	0.3180	− 7.56	− 1.27	6.29
						DCM	3.1952	0.3130	− 7.52	− 1.13	6.39
						DMSO	3.2156	0.3110	− 7.52	− 1.09	6.43
						Ethanol	3.2201	0.3106	− 7.51	− 1.07	6.44
TM4	3.08	0.32	− 7.60	− 1.43	6.17	Acetonitrile	3.1210	0.3204	− 7.32	− 1.08	6.24
						Benzene	3.0737	0.3253	− 7.40	− 1.25	6.15
						DCM	3.1050	0.3221	− 7.33	− 1.12	6.21
						DMSO	3.1199	0.3205	− 7.32	− 1.08	6.24
						Ethanol	3.1251	0.3200	− 7.32	− 1.07	6.25

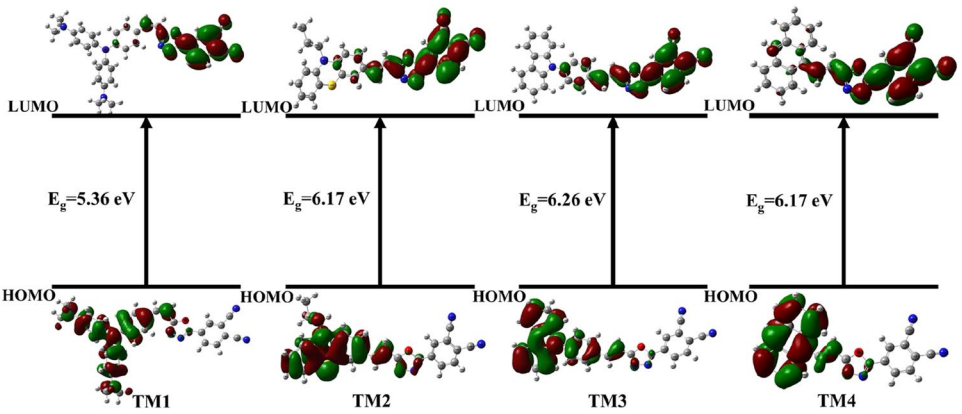

Fig. 2 Frontier molecular orbitals for $\pi \rightarrow \pi^*$ interactions calculated at ωB97XD/6–311 + + G (d, p) in gas phase

hyperpolarizability of TM4 is the lowest among the four molecules, which can be attributed to its structure and low contribution of charges.

FMO

The HOMO and LUMO, known as frontier molecular orbitals, are widely utilized for assessing the electronic and optical properties of molecules. They provide essential information regarding the spectroscopic and chemical characteristics of molecules [44, 45]. The stability of the molecule is linked to the energy variances of its orbitals. This information, presented in Table 5, along with the molecule's electronic structure (Fig. 2), aids in evaluating its diverse chemical properties. Here, we have calculated the HOMO–LUMO band gap energies of the TM1–TM4 chromophores at ground state, which are listed in Table 5 and depicted in Fig. 2, showing the FMO for $\pi \rightarrow \pi^*$ transitions computed for the ground state of the compounds. Frontier molecular orbitals with energy values closely situated to one another exhibit exceptionally polarizable characteristics, as indicated by the negative charge phase (red) and positive charge phase (green) patterns, suggesting their high reactivity. The HOMO covers the oxadiazole group, while the LUMO extends beyond it, indicating an electrophilic or nucleophilic region, facilitating attainable intramolecular interactions. Given the similar patterns and small energy gaps exhibited by all the molecules, it is probable that they are highly reactive. Furthermore, chemical parameters such as chemical hardness, reactivity, and softness of the molecules were computed using the HOMO–LUMO and are listed in Table 5.

Chemical hardness is a measure of a chemical species' resistance to changes in its electronic configuration, indicating the stability and electronegativity of its atoms [46, 47]. The chromophores TM1–TM4, listed in Table 5, provide the values of chemical hardness and chemical softness, which are obtained using Eqs. (4) and (5).

$$\eta = \frac{1}{2}\left[E_{\mathrm{LUMO}} - E_{\mathrm{HOMO}}\right] \tag{4}$$

$$\sigma = \frac{1}{\eta} \tag{5}$$

The HOMO–LUMO band gap exhibits a very low value, leading to softness in nature and high chemical reactivity, along with aromatic and polarizable properties [48]. This low bandgap energy of conjugated chromophores makes them highly suitable for potential optoelectronic applications. Additionally, chemical softness, which is the opposite of hardness, denotes the capacity to attract electron flow. It is associated with a polarizability attribute and can be calculated using Eq. 5. Softness is closely linked to the polarizability of the system, implying that a more polarizable chemical system is expected to be softer [49, 50].

NBO

The natural bond orbital (NBO) tool is utilized to analyze both intra- and inter-molecular interactions, providing valuable insights into the interactions of filled and virtual orbitals. It allows for the precise determination of a molecule's Lewis structure by maximizing the electron density percentage of an orbital [51–53]. Furthermore, it facilitates the extraction of data on variations in charge densities of donor and acceptor protons, particularly in bonding and antibonding orbitals. The tool also calculates intra-molecular charge transfer and determines effective interactions between the Lewis-type occupied NBO orbital (bonding) and non-Lewis unoccupied NBO orbital (anti-bonding) using the same level theory in both gas and solvent phases with detailed results presented in Table 6 as well as Tables S1, S2, and S3 from Supplementary Information. Another useful aspect is that it provides information about interactions in both filled and virtual orbital spaces which enhances analysis of intra- or inter-molecular interactions. Delocalization of electron

Table 6 Some selected most effective second-order perturbation (E2) transitions of TM1 chromophore are listed for evaluation of hyperconjugation energies (kcal/mol) calculated at ωB97XD/6–311 + + G(d, p)

Donor (*i*)	Type	ED(*e*)	Acceptor (*j*)	Type	ED(*e*)	*E* (2)*a* (kJ/mol)	*E*(*j*) − *E*(*i*)	*F* (*i*, *j*)
N1	σ	1.72849	C2	σ*	0.94567	100.80	0.20	0.154
	-	1.72849	C2-C3	-	0.02522	0.93	0.95	0.028
	-	1.72849	C2-C4	-	0.02460	0.89	0.95	0.028
	-	1.72849	C8-C9	-	0.02730	5.04	0.98	0.067
	-	1.72849	C8-C9	π*	0.39332	12.45	0.39	0.064
	-	1.72849	C8-C10	-	0.02775	5.11	0.98	0.067
	-	1.72849	C14-C15	-	0.02661	5.01	0.95	0.066
	-	1.72849	C14-C16	-	0.02731	4.89	0.98	0.066
	-	1.72849	C14-C16	π*	0.39546	12.21	0.39	0.064
N20	σ	1.76074	C10-C12	π*	0.34755	0.65	0.40	0.015
	-	1.76074	C11-C13	-	0.41768	51.31	0.39	0.133
N21	σ	1.76116	C15-C17	π*	0.34492	0.68	0.40	0.015
	-	1.76116	C18-C19	-	0.41771	51.23	0.39	0.132
O29	σ	1.97037	C28-N30	σ*	0.03072	4.70	1.30	0.070
	-	1.97037	C31-N32	-	0.28503	4.66	1.36	0.071
	-	1.97037	C31-C33	-	0.03385	0.54	1.23	0.023
	π	1.71322	C28-N30	π*	0.31229	46.09	0.48	0.133
	-	1.71322	C31-N32	-	0.28503	49.86	0.49	0.139
	-	1.71322	C41-N42	δ*	0.05802	1.24	0.89	0.032
N30	σ	1.93044	C28-O29	σ*	0.05094	12.14	0.89	0.093
	-	1.93044	C31-N32	-	0.03385	5.26	1.14	0.070
N32	σ	1.93858	C2	σ*	0.94567	1.15	0.38	0.027
	-	1.93858	N21-C25	-	0.01434	4.09	0.91	0.055
	-	1.93858	C33-C34	-	0.02190	0.96	1.05	0.029
C4-C6	σ	1.97153	N1-C2	σ*	0.03746	4.41	1.33	0.068
C6-C7	σ	1.96775	C5-C7	σ*	0.02146	4.28	1.40	0.069
C8-C9	σ	1.97143	C10-C12	σ*	0.01306	39.69	0.39	0.112
C9-C11	σ	1.97465	N1-C8	σ*	0.03886	4.83	1.29	0.071
C10-C12	π	1.71717	C11-C13	π*	0.41768	33.03	0.39	0.105
N21-C25	σ	1.98823	C35-C37	π*	0.26945	2007.65	0.22	0.637
O29-C31	σ	1.98979	C35-C37	π*	0.26945	10.09	0.04	0.019
N30-N32	σ	1.97111	C35-C37	π*	0.26945	839.75	0.36	0.521
C31-C33	σ	1.99091	C33-C35	σ*	0.02309	1077.94	0.09	0.278
C33-C35	σ	1.96730	C33-C35	σ*	0.02309	3652.23	0.12	0.585
C37-C38	σ	1.96739	C38-C41	σ*	0.02966	2835.47	0.09	0.457
C38-C41	σ	1.97928	C33-C35	σ*	0.02309	417.04	0.16	0.232
C41-N42	π	1.98764	C33-C35	σ*	0.02309	2664.19	0.09	0.447
C28-N30	π	1.86608	C26-C27	π*	0.17130	55.20	0.05	0.097
C33-C34	π	1.61998	C38-C41	σ*	0.02966	394.67	1.91	1.789
C35-C37	π	1.63135	C33-C35	σ*	0.02309	792.02	0.29	1.116
C36-C38	π	1.64732	C37-C38	π*	0.02308	1493.61	17.48	9.454
C36-C38	π	1.64732	C41-N42	δ*	0.05802	38.06	22.68	1.658

* symbol represents antibonding orbital representation

density between occupied NBO (bond or lone pair) and unoccupied NBO corresponds to stabilizing donor–acceptor interaction can be observed with estimation possible through second-order perturbation theory. Furthermore, conducting second-order perturbation theory on molecules allows for the calculation of stabilization energy using Eq. (6) [54].

$$E^{(2)} = q_i \frac{F^2(i,j)}{\varepsilon_j - \varepsilon_i} \tag{6}$$

where F^2 (i,j) represents the off-diagonal matrix elements, q_i gives the donor orbitals occupancy, ε_j and ε_i provide the values of donor and acceptor orbital energies, and $E^{(2)}$

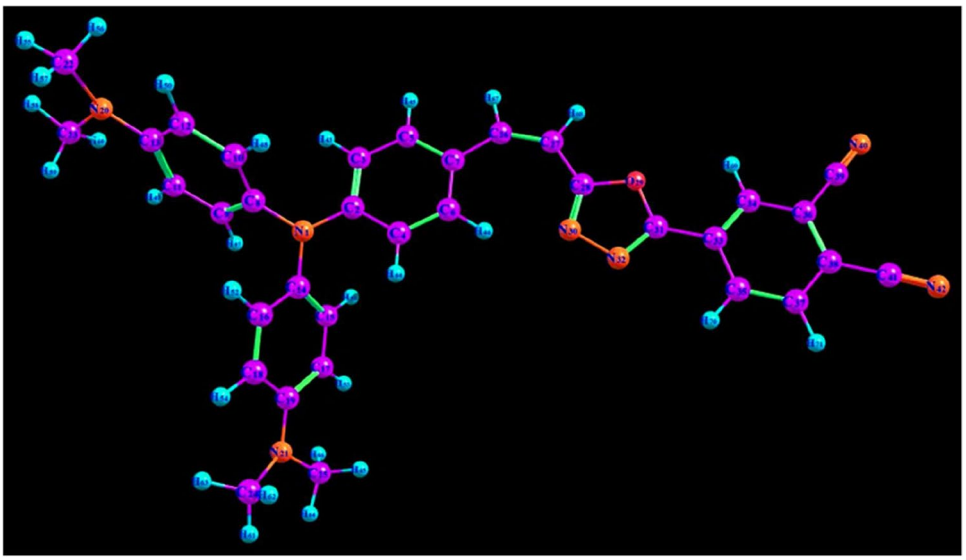

Fig. 3 Schematic charge in flow in molecule TM1

estimates the magnitude of the interaction between the donor and acceptor orbitals. There are different types of electronic transitions, in that four different typical electronic transitions are observed $\sigma \rightarrow \sigma^*$, $\pi \rightarrow \pi^*$, $LP \rightarrow \sigma^*$, and $LP \rightarrow \pi^*$ The most significant electronic transitions are found as among the above-mentioned transitions, while is examined as $\pi \rightarrow \pi^*$ are the least prominent, $LP \rightarrow \sigma^*$ and $LP \rightarrow \pi^*$ and $\sigma \rightarrow \sigma^*$are noticed as slightly dominant transitions. In the case of chromophore TM1 (Fig. 3), the most striking $\sigma \rightarrow \sigma^*$ transitions are C33–C35 and C37–C38, with stabilization energies at 3652.23 and 2835.47 kcal mol^{-1}, respectively. Examining the weaker transitions, significant values are also observed at 4.28 and 4.41 kcal mol^{-1} for transitions C6–C7 and C4–C6, respectively. Notable resonance transitions for discussion include N20 → C2, which shows the highest stabilization energy of 100.80 kcal mol^{-1}, and N20 → C10–C12, exhibiting the lowest stabilization energy of 0.65 kcal mol^{-1} (Table 6). The most effective transitions are observed at 3652.23 kJ/mol, 2001.29 kJ/mol, 2414 kJ/mol, and 2016.45 kJ/mol in TM1, TM2, TM3, and TM4, respectively. Additionally, two types of donors and three types of acceptors are observed, with the $\pi \rightarrow \pi^*$ transitions in both molecules contributing to high polarization, further influencing the NLO activity of the molecule.

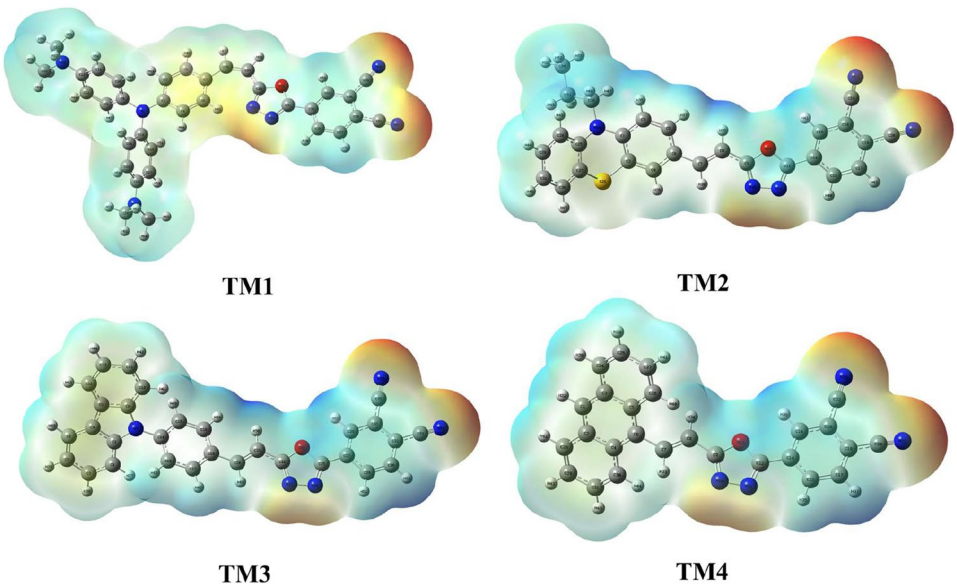

Fig. 4 Electrostatic potential surface TM1–TM4 obtained at ωB97XD/6–311 + + G (d, p)

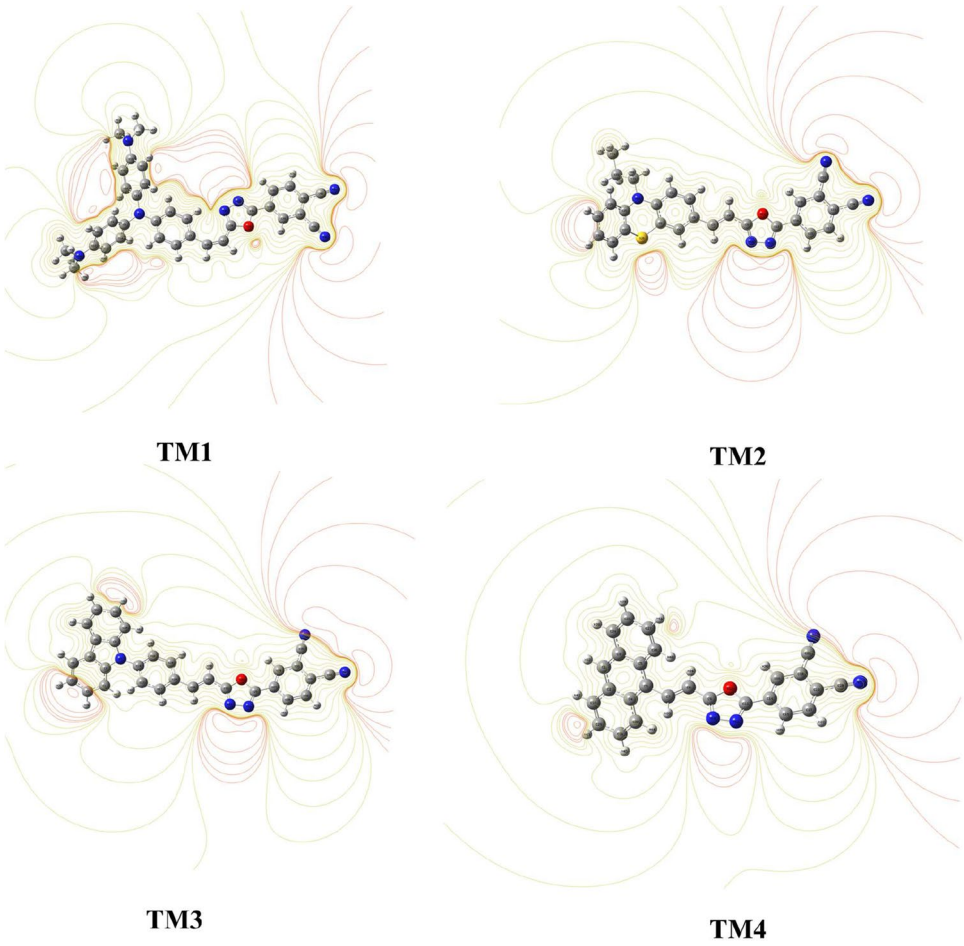

Fig. 5 Electrostatic potential Curve TM1–TM4 obtained at ωB97XD/6–311 + + G (d, p)

MEP

The molecular electrostatic potential (MEP) surfaces are essential in the field of optoelectronics, as they help analyze and understand the electronic structures of organic materials. The distribution of electron density around these molecules is crucial for understanding their reactive behavior. MEP maps use color gradation to display a molecule's size, structure, and positive, negative, and neutral electrostatic potential areas. These maps can identify regions where charged reagents will electrophilically attack organic compounds. Figure 4 depicts theoretical maps showing the distribution of electrostatic potential on the base ring plane obtained using density functional theory with a level basis set. Additionally, Fig. 5 presents a three-dimensional representation indicating positive nucleophilic sites (in blue), proton-rich electrophilic sites (in red), and electrically neutral regions (in white). The electrophilic cloud predominantly exists on oxygen and nitrogen atoms, encompassing groups such as 1,3,4-oxadiazole. In contrast, the nucleophilic cloud regions extend through the donor region surrounding hydrogen atoms like triphenylamine and carbazole [26]. Notably, the extension around the oxadiazole group has shown a strong positive charge while triphenyl amine exhibits a negatively charged region which signifies intramolecular charge transfer-based dipole moment orientation.

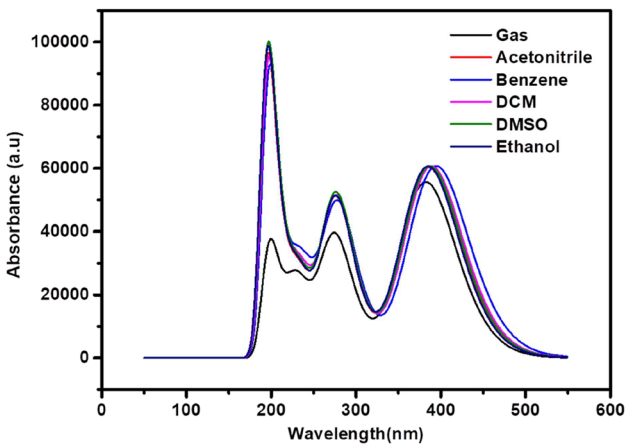

Fig. 6 UV–Vis spectrum of TM1 recorded at ωB3LYP/6–311 + + G (d, p) with $n = 50$ (n is number of excited states and wavelength in nm)

Table 7 UV–Vis spectrum, oscillator strength recorded at ωB3LYP/6–311 + + G (d, p) with $n = 50$ (n is the number of excited states)

Compound	TM1	TM2	TM3	TM4		TM1	TM2	TM3	TM4
Wavelength (nm)	382.4609501	349.07	333.57	376.28	Acetonitrile	385.76	353.52	332.41	380.34
					Benzene	394.81	358.61	339.33	385.43
					DCM	389.12	355.61	334.75	382.31
					DMSO	387.36	354.78	333.56	381.7
					Ethanol	385.19	353.1	332.32	380.18
Oscillator strength	1.370904024	1.1575	1.5435	0.4499	Acetonitrile	1.4857	1.3855	1.8557	0.5081
					Benzene	1.4977	1.3913	1.8012	0.5481
					DCM	1.4957	1.3978	1.8516	0.5252
					DMSO	1.4968	1.4058	1.8694	0.5202
					Ethanol	1.4942	1.3909	1.8608	0.5085

UV–Vis spectrum

The UV–Vis absorbance spectra provide valuable insights into the conjugation, transitions, and the nature of charge transfer processes in organic molecules [55]. It is worth noting that all the chromophores TM1–TM4 exhibit absorption maxima (λ_{max}) within the ultraviolet region (Fig. 6 and Figs. S1, S2, and S3).

UV–visible spectra were obtained using the TD-DFT method in DMSO, resulting in an enhanced value. Chromophores with donor functional groups containing delocalized π electrons typically exhibit electronic transitions of the $n \rightarrow \pi^*$ and $\pi \rightarrow \pi^*$ types. As shown in Fig. 6, TM1 exhibits absorption at λ_{max} in the ultraviolet region due to the presence of the 1,3,4-oxadiazole ring in the molecule's structure. The extended aromatic structure reduces the HOMO–LUMO gap, leading to a shift in the wavelength [56]. The oscillator strength indicates the effective number of electrons involved in transitions from the ground state to the excited state, resulting in the absorption area in the spectrum. Smaller oscillator strength leads to new transitions, as reflected in the oscillator strength values mentioned in Table 7. These values were found to be in the range associated with the solvents ethanol, DMSO, DCM, benzene, and acetonitrile, and were correlated with the hyperchromic effect of the TM1 sample in the solvent.

Overall, the investigation into the second-order nonlinear optical (NLO) properties of novel 1,3,4-oxadiazole derivatives, conducted through density functional theory (DFT), has yielded promising results that are indicative of their potential in various advanced optoelectronic applications. The study has successfully demonstrated that these derivatives exhibit significant NLO responses, which are highly desirable in the field for the development of efficient and compact optical devices specifically highlighting their utility in organic light-emitting diodes (OLEDs), photovoltaic cells, and as electro-optic modulators due to their promising second-order NLO properties. The theoretical framework provided by DFT has proven to be a powerful tool in predicting and understanding the electronic characteristics that govern the NLO behavior of these materials, laying a foundational basis for further experimental validation and application-driven research.

Conclusion

In conclusion, our study delved into the examination of second-order NLO properties in 1,3,4-oxadiazole derivative chromophores with various donor functional groups. The findings revealed significantly high hyperpolarizability and dipole moment values in TM1 and TM4 molecules when substituted with strong electron-donating groups such as triphenylamine and carbazole in DMSO solvent. Notably, TM1 demonstrated an exceptional first hyperpolarizability (β) of $293{,}679.0178 \times 10^{-34}$ esu alongside a dipole moment (μ) of 5.66 Debye and polarizability (α) of 110.62×10^{-24} esu when assessed in dimethyl sulfoxide (DMSO). Furthermore, under benzene solvent conditions utilizing ωB97XD functional with a basis set of 6–311 + + G(d,p), TM1 exhibited a low energy band gap measuring at 5.33 eV while NBO analysis confirmed the highest charge transfer value at E2 kJ/mol respectively. These molecules exhibit strong absorption maxima in the ultraviolet region and a lower HOMO–LUMO energy gap due to their aromatic structure. The derivatives also demonstrate good thermal stability, indicating the potential for enhancing nonlinear optical (NLO) response through structural tailoring with different electron-rich donor substituents. Moreover, the observed lower energy gap suggests possible intermolecular charge transfer within the π-conjugated molecular system, further supporting their promising NLO candidacy.

Supplementary Information The online version contains supplementary material available at https://doi.org/10.1007/s00894-024-05910-7.

Acknowledgements The authors express their thankfulness for the provision of computational facilities and Gaussian 16 under DST-FIST at the School of Chemical Sciences (formerly Department of Chemistry), Goa University. The authors gratefully thank Prof. Mahadevappa Y. Karidurаganavar and the Chairman, Department of PG Studies in Chemistry and Coordinator of Molecular Modelling Lab under the UPE FAR-I & DST PURSE Phase-II Programme at Karnatak University Dharwad, for providing the computational facility to the present work.

Author contributions Balachandar Waddar and Saidi Reddy Parne conceived and designed this project. Balachandar Waddar carried out the molecular simulations and drafted the manuscript. Suman Gandi and Vishnu Rama Chari discussed the simulation results and gave valuable suggestions. Saidi Reddy Parne and Guru Siddappa R. Prasanth supervised the molecular simulations and revised the manuscript. All authors approved the final version of the manuscript.

Data availability The datasets generated during and/or analyzed during the current study are available from the corresponding author upon reasonable request.

Declarations

Competing interests The authors declare no competing interests.

References

1. Wu J, Luo J, Jen AK-Y (2020) High-performance organic second- and third-order nonlinear optical materials for ultrafast information processing. J Mater Chem C 8(43):15009–15026
2. Dini D, Barthel M, Schneider T, Ottmar M, Verma S, Hanack M (2003) Phthalocyanines and related compounds as switchable materials upon strong irradiation: the molecular engineering behind the optical limiting effect. Solid State Ionics 165(1–4):289–303
3. Yahya M, Seferoğlu N, Barsella A, Achelle S, Seferoğlu Z (2021) Amino-substituted-1, 1-dicyano-2, 4-diaryl-1, 3-butadiene chromophores: Synthesis and photophysical properties. Spectrochim Acta Part A Mol Biomol Spectrosc 248:119178
4. Basu S (1984) A review of nonlinear optical organic materials. Ind Eng Chem Prod Res Dev 23(2):183–186
5. Liu F, Wang H, Yang Y, Xu H, Yang D, Bo S, Liu J, Zhen Z, Liu X, Qiu L (2015) Using phenoxazine and phenothiazine as electron donors for second-order nonlinear optical chromophore: enhanced electro-optic activity. Dyes Pigm 114:196–203
6. Liu J, Ouyang C, Huo F, He W, Cao A (2020) Progress in the enhancement of electro-optic coefficients and orientation stability for organic second-order nonlinear optical materials. Dyes Pigm 181:108509
7. Koos C, Vorreau P, Vallaitis T, Dumon P, Bogaerts W, Baets R, Esembeson B, Biaggio I, Michinobu T, Diederich F (2009) All-optical high-speed signal processing with silicon–organic hybrid slot waveguides. Nat Photon 3(4):216–219
8. Najare MS, Patil MK, Tilakraj TS, Yaseen M, Nadaf AA, Mantur S, Inamdar SR, Khazi IAM (2021) Photophysical and electrochemical properties of highly π-conjugated bipolar carbazole-1, 3, 4-oxadiazole-based d-π-a type of efficient deep blue fluorescent dye. J Fluoresc 31:1645–1664
9. Jia YJ, Chen YG, Guo Y, Guan XF, Li C, Li B, Liu MM, Zhang XM (2019) LiMII (IO3) 3 (MII= Zn and Cd): two promising nonlinear optical crystals derived from a tunable structure model of α-LiIO3. Angew Chem Int Ed 58(48):17194–17198
10. Marder SR, Perry JW, Tiemann BG, Marsh RE, Schaefer WP (1990) Second-order optical nonlinearities and photostabilities of 2-N-methylstilbazolium salts. Chem Mater 2(6):685–690
11. Waddar B, Parne SR, Gandi S, Prasanth GR, Yaseen M, Karidurаganavar MY (2023) The second-order nonlinear optical properties of novel triazolo [3, 4-b][1, 3, 4] thiadiazole derivative chromophores using DFT calculations. Struct Chem 35:253–264
12. Bella SD (2001) Second-order nonlinear optical properties of transition metal complexes. Chem Soc Rev 30(6):355–366
13. Bureš F, Čermáková H, Kulhánek J, Ludwig M, Kuznik W, Kityk IV, Mikysek T, Růžička A (2012) Structure–property relationships and nonlinear optical effects in donor-substituted dicyanopyrazine-derived push–pull chromophores with enlarged and varied π-linkers. Eur J Org Chem 2012(3):529–538
14. Kim TD, Lee KS (2015) D-π-A conjugated molecules for optoelectronic applications. Macromol Rapid Commun 36(11):943–958
15. Mishra A, Ma C-Q, Bauerle P (2009) Functional oligothiophenes: molecular design for multidimensional nanoarchitectures and their applications. Chem Rev 109(3):1141–1276
16. Pron A, Gawrys P, Zagorska M, Djurado D, Demadrille R (2010) Electroactive materials for organic electronics: preparation strategies, structural aspects and characterization techniques. Chem Soc Rev 39(7):2577–2632
17. Mikroyannidis JA, Spiliopoulos IK, Kasimis TS, Kulkarni AP, Jenekhe SA (2003) Synthesis, photophysics, and electroluminescence of conjugated poly (p-phenylenevinylene) derivatives with 1, 3, 4-oxadiazoles in the backbone. Macromolecules 36(25):9295–9302
18. Najare MS, Patil MK, Garbhagudi M, Yaseen M, Inamdar SR, Khazi IAM (2021) Design, synthesis and characterization of π-conjugated 2, 5-diphenylsubstituted-1, 3, 4-oxadiazole-based D-π-A-π'-D′ form of efficient deep blue functional materials: photophysical properties and fluorescence "Turn-off" chemsensors approach. J Mol Liq 328:115443
19. Najare MS, Patil MK, Nadaf AA, Mantur S, Garbhagudi M, Gaonkar S, Inamdar SR, Khazi IAM (2020) Photophysical, thermal properties, solvatochromism and DFT/TDDFT studies on novel conjugated DA-π-AD form of small molecules comprising thiophene substituted 1, 3, 4-oxadiazole. J Mol Struct 1199:127032
20. Oliveira MS, Santos AB, Ferraz TV, Moura GL, Falcão EH (2023) Non-symmetrical 1, 3, 4-oxadiazole derivatives: synthesis, characterization, and computational study of their optical properties. Chem Phys Impact 6:100162
21. Khemalapure SS, Hiremath SM, Hiremath CS, Katti VS, Basanagouda MM (2020) Investigations of structural, vibrational and electronic properties on 5-(6-methyl-benzofuran-3-ylmethyl)-3H-[1, 3, 4] oxadiazole-2-thione: experimental and computational approach. Chem Data Collect 28:100410
22. Alongamo CHA, Nkungli NK, Ghogomu JN (2019) DFT-based study of the impact of transition metal coordination on the charge transport and nonlinear optical (NLO) properties of 2-{[5-(4-nitrophenyl)-1, 3, 4-thiadiazol-2-ylimino] methyl} phenol. Mol Phys 117(18):2577–2592
23. Carella A, Castaldo A, Centore R, Fort A, Sirigu A, Tuzi A (2002) Synthesis and second order nonlinear optical properties of new chromophores containing 1, 3, 4-oxadiazole and thiophene rings. J Chem Soc Perkin Trans 2(11):1791–1795
24. Fang Y-K, Liu C-L, Chen W-C (2011) New random copolymers with pendant carbazole donor and 1, 3, 4-oxadiazole acceptor for high performance memory device applications. J Mater Chem 21(13):4778–4786
25. Homocianu M, Airinei A, Ipate AM, Hamciuc C (2022) Spectroscopic recognition of metal ions and non-linear optical (NLO) properties of some fluorinated poly (1, 3, 4-oxadiazole-ether) s. Chemosensors 10(5):183

26. Dhannur SH, Shridhar A, Suresh S, Al-Asbahi BA, Al-Hada NM, Shelar VM, Naik L (2024) DFT studies on D–π–A substituted bis-1, 3, 4-oxadiazole for nonlinear optical application. J Opt 1–11. https://doi.org/10.1007/s12596-024-01698-0
27. Homocianu M, Airinei A, Hamciuc C, Ipate AM (2019) Nonlinear optical properties (NLO) and metal ions sensing responses of a polymer containing 1, 3, 4-oxadiazole and bisphenol A units. J Mol Liq 281:141–149
28. Barbosa-Silva R, Oliveira MS, Ferreira RC, Manzoni V, Falcão EH, de Araújo CB (2023) Second-order optical nonlinearity of two 1, 3, 4-oxadiazole derivatives: an experimental and theoretical study. Opt Mater 146:114536
29. Kohn W, Becke AD, Parr RG (1996) Density functional theory of electronic structure. J Phys Chem 100(31):12974–12980
30. Kotteswaran S, Ramasamy P (2021) The influence of triphenylamine as a donor group on Zn–porphyrin for dye sensitized solar cell applications. New J Chem 45(5):2453–2462
31. Yang Y, Xu W, Zhao J, Liu J (2019) Using phenothiazine as electron donor for new second-order nonlinear optical chromophore. Mater Lett 245:196–199
32. Kukhta A, Kukhta I, Kukhta N, Neyra O, Meza E (2008) DFT study of the electronic structure of anthracene derivatives in their neutral, anion and cation forms. J Phys B: At Mol Opt Phys 41(20):205701
33. Huang Z, Gu Y, Liu X, Zhang L, Cheng Z, Zhu X (2017) Metal-free atom transfer radical polymerization of methyl methacrylate with ppm Level of organic photocatalyst. Macromol Rapid Commun 38(10):1600461
34. Garza AJ, Osman OI, Wazzan NA, Khan SB, Asiri AM, Scuseria GE (2014) A computational study of the nonlinear optical properties of carbazole derivatives: theory refines experiment. Theoret Chem Acc 133:1–8
35. Mahmood A, Khan SUD, Rana UA, Janjua MRSA, Tahir MH, Nazar MF, Song Y (2015) Effect of thiophene rings on UV/visible spectra and non-linear optical (NLO) properties of triphenylamine based dyes: a quantum chemical perspective. J Phys Org Chem 28(6):418–422
36. Ledwon P (2019) Recent advances of donor-acceptor type carbazole-based molecules for light emitting applications. Org Electron 75:105422
37. Blanchard P, Malacrida C, Cabanetos C, Roncali J, Ludwigs S (2019) Triphenylamine and some of its derivatives as versatile building blocks for organic electronic applications. Polym Int 68(4):589–606
38. Me F, Trucks G, Schlegel HB, Scuseria G, Robb M, Cheeseman J, Scalmani G, Barone V, Petersson G, Nakatsuji H (2016) Gaussian 16. Gaussian, Inc., Wallingford, CT
39. Marenich AV, Cramer CJ, Truhlar DG (2009) Universal solvation model based on solute electron density and on a continuum model of the solvent defined by the bulk dielectric constant and atomic surface tensions. J Phys Chem B 113(18):6378–6396
40. Jiang X, Zhao S, Lin Z, Luo J, Bristowe PD, Guan X, Chen C (2014) The role of dipole moment in determining the nonlinear optical behavior of materials: ab initio studies on quaternary molybdenum tellurite crystals. J Mater Chem C 2(3):530–537
41. Acemioğlu B, Arık M, Efeoğlu H, Onganer Y (2001) Solvent effect on the ground and excited state dipole moments of fluorescein. J Mol Struct (Thoechem) 548(1–3):165–171
42. Ahn M, Kim M-J, Cho DW, Wee K-R (2020) Electron push–pull effects on intramolecular charge transfer in perylene-based donor–acceptor compounds. J Org Chem 86(1):403–413
43. Parthasarathy V, Pandey R, Das PK, Castet F, Blanchard-Desce M (2018) Linear and nonlinear optical properties of tricyanopropylidene-based merocyanine dyes: synergistic experimental and theoretical investigations. ChemPhysChem 19(2):187–197
44. Drissi M, Benhalima N, Megrouss Y, Rachida R, Chouaih A, Hamzaoui F (2015) Theoretical and experimental electrostatic potential around the m-nitrophenol molecule. Molecules 20(3):4042–4054
45. Shimizu A, Ishizaki Y, Horiuchi S, Hirose T, Matsuda K, Sato H, Yoshida J-i (2020) HOMO–LUMO energy-gap tuning of π-conjugated zwitterions composed of electron-donating anion and electron-accepting cation. J Org Chem 86(1):770–781
46. Kaya S, Kaya C (2015) A new method for calculation of molecular hardness: a theoretical study. Comput Theor Chem 1060:66–70
47. Pearson RG (1990) Hard and soft acids and bases—the evolution of a chemical concept. Coord Chem Rev 100:403–425
48. Pegu D, Deb J, Van Alsenoy C, Sarkar U (2017) Theoretical investigation of electronic, vibrational, and nonlinear optical properties of 4-fluoro-4-hydroxybenzophenone. Spectrosc Lett 50(4):232–243
49. Gázquez JL (1993). Hardness and softness in density functional theory. In: Sen KD (ed) Chemical Hardness. Structure and Bonding, vol 80. Springer, Berlin, Heidelberg. https://doi.org/10.1007/BFb0036798
50. Domingo LR, Chamorro E, Pérez P (2008) Understanding the reactivity of captodative ethylenes in polar cycloaddition reactions A theoretical study. J Org Chem 73(12):4615–4624
51. Demircioğlu Z, Kaştaş ÇA, Büyükgüngör O (2015) Theoretical analysis (NBO, NPA, Mulliken Population Method) and molecular orbital studies (hardness, chemical potential, electrophilicity and Fukui function analysis) of (E)-2-((4-hydroxy-2-methylphenylimino) methyl)-3-methoxyphenol. J Mol Struct 1091:183–195
52. Sheela N, Muthu S, Sampathkrishnan S (2014) Molecular orbital studies (hardness, chemical potential and electrophilicity), vibrational investigation and theoretical NBO analysis of 4–4′-(1H–1, 2, 4-triazol-1-yl methylene) dibenzonitrile based on abinitio and DFT methods. Spectrochim Acta Part A Mol Biomol Spectrosc 120:237–251
53. Rizwana BF, Prasana JC, Muthu S, Abraham CS (2019) Spectroscopic (FT-IR, FT-Raman, NMR) investigation on 2-[(2-amino-6-oxo-6, 9-dihydro-3H-purin-9-yl) methoxy] ethyl (2S)-2-amino-3-methylbutanoate by density functional theory. Mater Today: Proc 18:1770–1782
54. Chocholoušová J, Špirko V, Hobza P (2004) First local minimum of the formic acid dimer exhibits simultaneously red-shifted O-H··· O and improper blue-shifted C–H··· O hydrogen bonds. Phys Chem Chem Phys 6(1):37–41
55. Gelfand N, Freidzon A, Vovna V (2019) Theoretical insights into UV–Vis absorption spectra of difluoroboron β-diketonates with an extended π system: an analysis based on DFT and TD-DFT calculations. Spectrochim Acta Part A Mol Biomol Spectrosc 216:161–172
56. Kariduraganavar MY, Doddamani RV, Waddar B, Parne SR (2021) Nonlinear optical responsive molecular switches. IntechOpen. https://doi.org/10.5772/intechopen.92675